King Saud University

Arabian Journal of Chemistry

www.ksu.edu.sa
www.sciencedirect.com

ORIGINAL ARTICLE

Adsorption characteristics of alumina nanoparticles for the removal of hazardous dye, Orange G from aqueous solutions

CrossMark

Sushmita Banerjee [a], **Shikha Dubey** [a], **Ravindra Kumar Gautam** [b],
M.C. Chattopadhyaya [b], **Yogesh C. Sharma** [a],*

[a] *Department of Chemistry, Indian Institute of Technology, Banaras Hindu University, Varanasi 221 005, India*
[b] *Environmental Chemistry Research Laboratory, Department of Chemistry, University of Allahabad, Allahabad 211 002, India*

Abstract   The application of nanomaterials for water treatment has gained impetus in recent years. Nano-adsorbents offer significant decontamination potential due to their unique characteristics. Present study deals with synthesis and application of alumina nanoparticles for removal of an anionic dye, Orange G (OG) from aqueous solutions. The properties of synthesized nanoparticles were investigated by FTIR, TG/DTA, XRD, TEM, SEM, EDX and N$_2$ adsorption-desorption techniques. The effect of various important parameters on dye removal was examined and adsorption was found to be highly pH dependent and maximum removal of 98.4% was observed at pH 2.5. The presence of interfering anions such as SO_4^{2-}, PO_4^{3-}, and $C_2O_4^{2-}$ was found to be limiting factor of the adsorption process. The kinetic results demonstrated that the sorption process was described by pseudo-second-order model. Mechanism of adsorption process was also interpreted with the help of diffusion models and the results exhibited that external diffusion governed the overall sorption process. The Langmuir model yielded a good fit for the experimental data with high adsorption capacity (93.3 mg/g at 303 K). The evaluated thermodynamic parameters ΔG°, ΔH° and ΔS°, proposed that adsorption of OG was spontaneous, feasible, and exothermic under investigated conditions. Desorption experiments confirmed that the exhausted adsorbent can be successfully regenerated and can be effectively reused up to four successive cycles with almost the same sorption capacity resulting in reducing cost of treatment. The adsorption performance of alumina nanoparticles was also tested by using real wastewater and results indicated that nano alumina is proficient for the treatment of multi-solute system also.

---

* Corresponding author. Fax: +91 542 6702876.
   E-mail address: ysharma.apc@itbhu.ac.in (Y.C. Sharma).

Production and hosting by Elsevier

1. Introduction

The advent of technology based on harnessing the potential of nanoscale materials has revolutionized the field of material science. There is growing interest in nanoscience which indicates that there are many aspects in the related fields that are still unexplored and yet to be addressed (Tang et al., 2015; Li et al., 2015; Malgras et al., 2015; Malgras et al., 2016). In nanoscience, the most imperative aspect is the fabrication of materials having dimensions in the order of 1/100 nm or less. In recent years, the use of nanotechnology in environmental applications for wastewater treatment has gained significant attention (Brame et al., 2011). Nanoscale materials in water treatment have produced tremendous performances which may be attributed to their unique characteristics such as high surface area to volume ratio, small size, availability of large number of reactive sites, and a high capacity for regeneration (Ali, 2012). The current water pollution based problems, including water quality, can be ameliorated using nanoadsorbents, nanocatalysts, nanostructured catalytic membranes, and many more products and processes resulting from the advancement of nanotechnology (Savage and Diallo, 2005). A large number of nanomaterials have been synthesized and employed as adsorbents for separation of pollutants from the liquid phase (Mohmood et al., 2013). Among the inorganic nanomaterials, iron and aluminum based nanoscale adsorbent materials (Li et al., 2006; Sharma et al., 2008; Sharma et al., 2009; Hordern, 2004; Giles et al. 2011) were the first to be investigated which may be due to the low manufacturing cost and high decontamination efficiency. Nano-alumina is one of the most important and extensively explored ceramic materials widely used as catalysts or catalyst supports for chemical reactions, electrical insulators, structural composites for spacecraft, abrasive and thermal wear coatings, membrane applications as well as adsorbent for water and wastewater treatment (Sharma et al., 2010; Srivastava et al., 2011; Yalamaç et al., 2014; Cai et al., 2015). Alumina is reported to exist in several phases (Shek et al., 1997) but its gamma phase has been highly desirable because of its superior micro-structural properties and enhanced thermodynamic stability after attaining a critical surface area (Zhou et al., 2007). So far, several methods have been reported for the preparation of γ-alumina nanocrystals (Zhou et al., 2007; Tok et al., 2006; Bahaabad and Nassaj 2008; Li et al., 2009; Renuka et al., 2012). Each of the reported methods has its own limitation such as complex synthesis procedure, high cost of starting materials, toxic precursors, requirement of high energy input, large grain size, not viable for large scale production and low yield. Therefore, in order to overcome the limitations, "ethanol mediated sol-gel precipitation route" a simple, cost-effective and environmentally friendly technique has been adopted for the synthesis of γ-alumina nanocrystals. The sol-gel process has many advantages such as high phase purity, good compositional homogeneity, and a high surface activity of the resulting synthesized powders (Shao et al., 2012).

In the present investigation, the γ-alumina nanocrystals were synthesized and used for the adsorptive removal of a toxic dye, Orange G (OG) from its aqueous solutions. OG is a monoazo, negatively charged dye and is widely used in printing and textile industries. The dye is reported to be highly toxic to human beings due to its carcinogenic and teratogenic nature. The study deals with the adsorptive removal of OG from aqueous solutions using batch adsorption technique. The investigation and optimization of various process variables influencing the removal process were carried out. Kinetics, isotherm and thermodynamic studies were carried out for a better understanding of the adsorption process. The scope for adsorbent regeneration was also explored in order to make the treatment process cost-effective and finally an industrial wastewater was tested.

2. Materials and methods

2.1. Chemicals and reagents

All the reagents used in the synthesis were of analytical (a. r.) grade with the mass fraction purity of 0.99 and were used as received without any further purification. $AlCl_3 \cdot 6H_2O$ was purchased from Alfa Aesar, England and Orange G from E. Merck, Mumbai, India. Highest purity analytical reagent grades of liquid ammonia and ethanol (95%), HCl and NaOH were supplied by E. Merck, Mumbai, India. The stock solutions of Orange G were prepared by dissolving 1.0 g of dye in 1000 mL of double distilled water and working solutions of 50, 75, 100 and 125 mg/L were prepared daily with the required dilution.

2.2. Synthesis of alumina nanoparticles

γ-phase alumina nanoparticles were synthesized using the sol-gel precipitation in ethanol process as reported by Wang et al. (2008) with little modification. A precursor solution of 0.6 M was prepared using $AlCl_3 \cdot 6H_2O$ dissolved in ethanol (95%). The precipitating agent, liquid ammonia (1.0 M) was added dropwise to the ethanol solution with continuous stirring and this resulted in formation of a gelatinous white precipitate of $Al(OH)_3$. The resultant precipitate was filtered and washed with ethanol followed by oven drying at 90 °C for 6 h. The dried white gel was calcined in a muffle furnace at 600 °C for 3 h in the presence of air at a heating rate of 10 °C/min, thus transforming $Al(OH)_3$ into Al_2O_3 powder. After calcination, the calcined powder was milled and sieved. A yield of 91% was obtained. The advantage of ethanol based precipitation over aqueous precipitation is that in the former case, particles were formed having high degree of dispersivity due to formation of soft agglomerates, while in the latter case, hard heavy agglomerates were formed due to chemical interaction of absorbed water molecules with surface hydroxyl groups between adjacent particles.

2.3. Characterization of the adsorbent

The FTIR spectra of as-synthesized material were recorded on a Fourier Transform Infrared Spectrophotometer (Varian 1600 FT-IR Scimitar Series) to identify the functional groups present on the adsorbent. For recording IR spectra, the sample was encapsulated in KBr using a hydraulic pellet press and the spectra were taken in the wavelength range from 4000 cm^{-1} to 400 cm^{-1} with a resolution of 4 cm^{-1}. The TG/DTA was performed in a Simultaneous Thermal Analysis System (NETZSCH STA 409 PC/PG). The sample, mass 11 mg, was heated at a scanning rate of 10 °C/min under dynamic N_2 flow of 75 mL/min at temperature range 31 °C to 1000 °C. The X-ray diffraction pattern of the adsorbent was recorded by an X-ray diffractometer (XPERT-PRO) operated at 45 kV/40 mA using CuKα radiation with wavelength of 1.54 Å and a scanning rate of 1° per min. The crystallite size was evaluated from the diffraction peaks by using the Scherrer method. The adsorbent size was further assessed by analyzing the images recorded by a Transmission Electron Microscope (Philips CM200) at an accelerating electron voltage of 200 kV. Samples for TEM analysis were prepared by introducing a drop of suspension over a copper grid. The surface feature and elemental composition of the as-synthesized material were determined by Scanning Electron Microscope (Zeiss, Germany) and Energy Dispersive X-ray Spectroscopy at an accelerating voltage of 15.0 kV. The textural properties of the adsorbent were determined by N_2 adsorption-

desorption isotherms measured at $-196\,°C$ using specialized analyzer (ASAP 2020, Micromeritics, USA). Prior to analysis, the sample was degassed at $250\,°C$ for 2 h in the degas port of the analyzer. The adsorption data in the P/P_0 range of 0.01–0.18 were used to calculate the specific surface area of the product by the Brunauer−Emmett−Teller (BET) method. The pore size distribution was analyzed with the help of desorption curve of the isotherm through Barrett−Joyner−Hallenda (BJH) method.

2.4. Determination of pH$_{ZPC}$ (point of zero Charge)

pH$_{ZPC}$ of an adsorbent is an important characteristic as it helps in determining the pH value at which the surface of the adsorbent becomes electrically neutral and facilitates in predicting the surface behavior of adsorbent materials. For determination of pH$_{ZPC}$, the solid addition method was adopted using 0.01 M NaCl. The solution was placed in six different flasks: each containing 200 mg of alumina nanoparticles at different pH values. The pH of the solutions was adjusted in 2.0–12.0 range by using NaOH and HCl solutions. The flasks were then agitated at 120 rpm for 24 h and the pH of the solutions was measured by a pH meter (Systronics 335). A graph of pH$_{final}$ vs. pH$_{initial}$ was plotted and the point of intersection of the two graphs represents the pH$_{ZPC}$ of the alumina nanoparticles.

2.5. Batch adsorption experiments

A series of batch adsorption experiments was carried out to investigate the optimum operating conditions for adsorption of OG on alumina nanoparticles. The effect of important process variables including initial dye concentration, contact time, solution pH and temperature was studied using 100 mL of dye solution in 250 mL Erlenmeyer conical flasks. In all adsorption experiments, 0.1 g of adsorbent was added. The mixture was agitated at 200 rpm for the desired time in a shaking thermostatically controlled water bath (Macro Scientific Works Pvt. Ltd., Delhi) at 303 K. The samples were collected from the flasks at regular intervals followed by centrifugation. The residual dye concentration in the supernatant was determined by UV-visible spectrophotometer (Model-2203, Systronics, Ahmadabad, India) at 480 nm. The percentage removal of OG and adsorption capacity (q_e) of alumina nanoparticles were calculated using the following equation:

$$\%Removal = \frac{C_0 - C_e}{C_0} \times 100 \tag{1}$$

$$q_e = \left(\frac{C_0 - C_e}{W}\right) V \tag{2}$$

where q_e is the amount of dye adsorbed at time of equilibrium (mg/g), C_0 and C_e are initial and final concentration of dye (mg/L), V (L) is the volume of sample, and W (g) is the mass of adsorbent. For kinetic investigations, residual dye concentrations for different initial concentrations were analyzed, keeping other operating parameters such as pH, temperature and adsorbent dose constant. The samples were collected at regular time intervals of 5 min up to the equilibrium period for the analysis purpose. The adsorption isotherm experiments were carried out using various initial dye concentrations at

different temperatures keeping pH, sorbent dose, etc. constant and agitated until the attainment of equilibrium.

Blank experiments were carried out using 100 mg/L dye solution in a flask without adsorbent to ensure that no dye was adsorbed onto the walls of flasks, while another experiment was conducted using adsorbent and water only to check the sorbent leaching issue which may interfere with the measurement of dye concentrations during spectroscopic analysis.

In order to maintain accuracy, batch experiments were replicated to ensure reproducibility of obtained data. Each batch adsorption experiment was performed in triplicate producing results with deviations $<5\%$. If the error was found to be $>5\%$, another set of experiments was performed. The data of the batch experiments used for the experimental analysis were the average values of three tests.

2.6. Error analysis

An error function assessment is required in order to avoid the biased result that usually occurs due to use of linear expressions resulting from the transformation of nonlinear expressions. Therefore, in the present study, the quality of fit was verified and quantitatively compared with the applicability of other models through the coefficient of determination (R^2) and hybrid fractional error function (HYBRID) (Porter et al. (1999):

$$\frac{100}{n-p} \Sigma_{i=1}^{n} \left[\frac{(q_{e,exp} - q_{e,calc})^2}{q_{e,exp}}\right] \tag{3}$$

The error function represents the ameliorated version of the sum of squares of the errors (ERRSQ) fit at low concentration. Accordingly, each ERRSQ value is divided by experimental $q_{e,exp}$, values. This function also includes the number of degrees of freedom of the system which can be evaluated as the number of data points, n, minus the number of parameters, p, of the isotherm equation—as a divisor.

2.7. Desorption and regeneration experiments

To evaluate the reusability of the adsorbent, the adsorption of Orange G and the regeneration of dye loaded alumina nanoparticles were performed by repeating adsorption–desorption cycles five times. In each cycle, 50 mg/L of 100 mL dye solution was mixed with 0.1 g of sorbent for equilibrium period. The loaded sorbents were separated through centrifugation and the supernatant dye solutions were analyzed. The resultant loaded sorbent was tested with different desorbing solutions such as 0.1 M HCl, 0.1 M HClO$_4$, 0.1 M HNO$_3$, 0.1 M H$_2$SO$_4$, and 0.1 M H$_3$PO$_4$ in order to examine the efficiency of each solution toward desorption. Prior to the next adsorption–desorption cycle, the regenerated sorbent was washed thoroughly with distilled water to pH–7.0.

2.8. Stability test

In order to evaluate the stability of the alumina nanoparticles, the leaching of aluminum ions from the adsorbent at variable pH conditions was investigated. Experiments were conducted by dispersing 0.1 g of alumina nanoparticles in 100 mL of aqueous solution with pH values ranging from 2.5 to 9.5. The resultant solutions were kept for shaking in a temperature-controlled

shaker at 303 K for 120 min. The concentration of leached aluminum ions in the supernatant was quantified by atomic absorption spectroscopy (AA7000, Shimadzu, Japan).

3. Results and discussion

3.1. Characterization of alumina nanoparticles

The assessment of the surface functional groups of the adsorbent material was carried out by FTIR spectrum analysis (Fig. 1). In the fresh sample (Fig. 1aA), the presence of the prominent peak at 3457 cm^{-1} is attributed to the stretching vibration of the —OH group from Al—OH framework and another peak at 1629 cm^{-1} is ascribed to physically adsorbed water molecules

(Yang et al., 2010). The presence of a wide pattern extending in 400–1000 cm^{-1} range substantiates the formation of γ-phase alumina. The absorption bands at 911, 804 and 637 cm^{-1} correspond to asymmetric stretching, symmetric stretching and bending vibration of the Al—O—Al bond (Afkhami et al., 2010), respectively. The presence of peaks below 700 cm^{-1} is related to an octahedral arrangement of Al^{3+} ions in the hcp lattice of the oxide ions while peaks between 700 and 950 cm^{-1} indicate the occupancy of Al^{3+} ions in the tetrahedral sites in the ccp lattice of the oxide ions (Busca et al., 1993). Therefore, the as-synthesized γ-phase alumina comprises both octahedral and tetrahedral coordination units. Fig. 1aB represents adsorbent material after the sorption of dye ions. It can be clearly noticed that after dye adsorption, there has been slight change in peak positions. The peak intensity band at 3457 cm^{-1} was
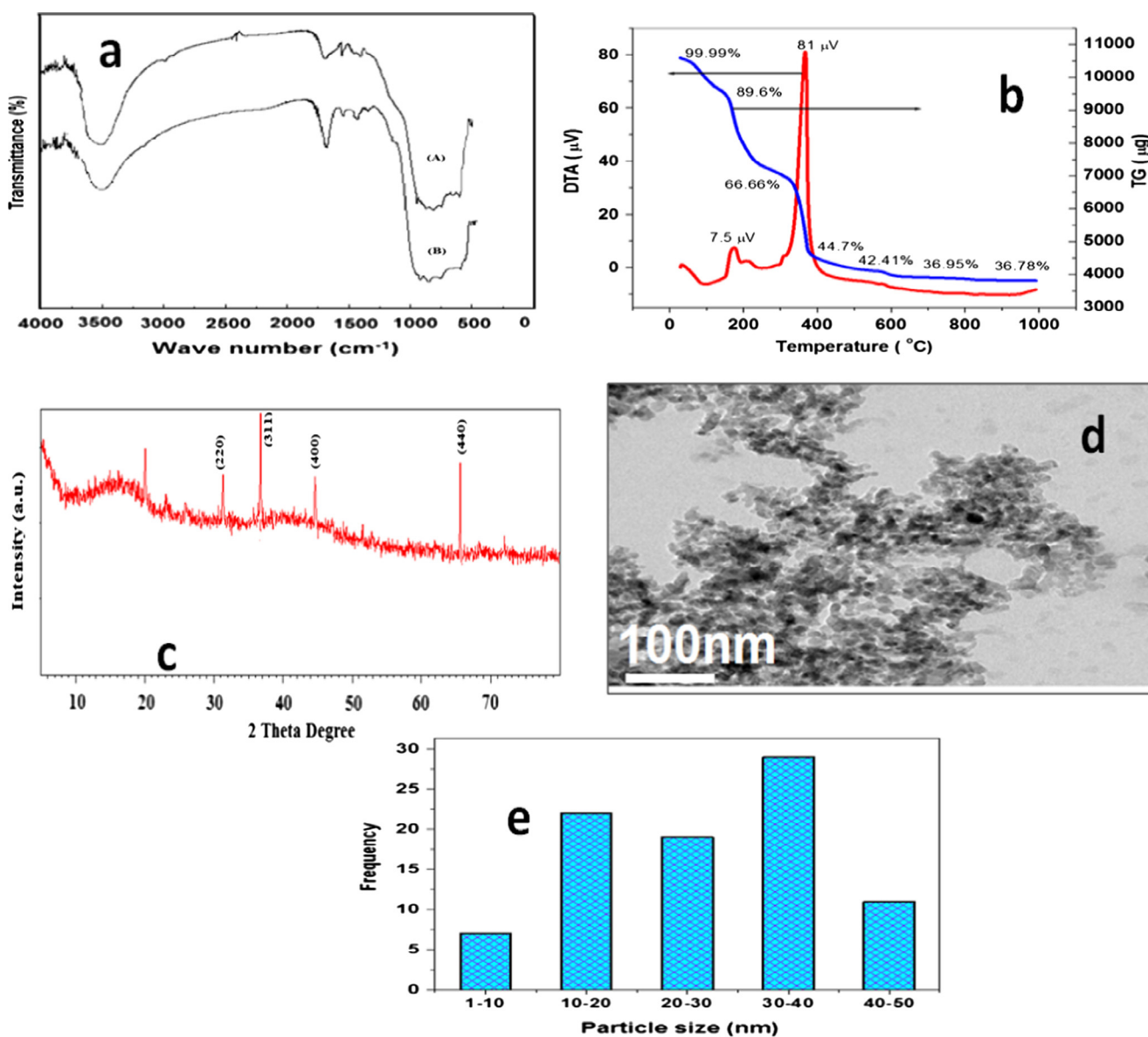

Figure 1 a: FTIR of fresh and dye loaded alumina nanoparticles; b: TG/DTA of alumina nanoparticles; c: XRD diffraction patterns; d: TEM image of alumina nanoparticles; e: particle size distribution analysis of alumina nanoparticles.

found to be reduced slightly and a small shift in peak position was observed in the absorption band 1000–400 cm^{-1}. This indicates that dye ions most probably interact with Al—OH and Al—O groups present on the adsorbent surface.

The thermal behavior of the sample has been studied by TG-DTA analysis (Fig. 1b). The TG curve of the sample exhibited three weight losses. The first weight loss amounts to *ca* 11% of the initial sample weight and terminates at ~148 °C, and this weight loss corresponds to a well distinguished exothermic peak in the DTA profile. This peak represents desorption of physically adsorbed water (Shen et al. 2012). The second significant weight loss of about 34% is recorded between 150 and 300 °C, which may be attributed to elimination of ethanol and impurities. The third weight loss can be observed at 375 °C and accounts for nearly 65% weight loss with a prominent exothermic peak observed in the DTA pattern ascribed to the dehydration of amorphous aluminum hydroxide (Isfahani et al., 2012). Beyond 600 °C, no significant weight loss is observed and the material becomes thermally stable. Hence, the sorbent was calcined at this temperature in order to obtain γ-phase alumina particles.

The phase confirmation of the as-synthesized adsorbent was accomplished through investigating the X-ray diffractogram as shown in Fig. 1c. The diffractogram clearly indicates the amorphous nature of the sample. The four characteristic reflections at 2θ = 32°, 37.4°, 45.2° and 67.5° with corresponding reflection planes of 220, 311, 400 and 440 reveal the formation of the γ-species. The obtained peaks were also found to be in good agreement with the standards' database (JCPDS card 00-029-0063) (Huang et al., 2013). Besides phase confirmation, the diffraction peaks were also inspected for the determination of the particle size of the as-synthesized material by using Scherrer formula (Patterson, 1939):

$$d = 0.9\lambda/fwhm\cos\theta \qquad (4)$$

where d is the crystallite size (nm), λ is the wavelength of the monochromatic X-ray beam (nm), (λ is 0.154056 nm for CuKα radiation), fwhm is the "full-width at half-maximum" for the diffraction peak under consideration (rad), and θ is the Bragg angle (deg). The results derived from the (220), (311), (400) and (440) reflections were being averaged. The average crystallite size of alumina particles was evaluated as approximately 28 nm.

The morphological aspects and the diameter of the nanoparticles were ascertained through TEM analysis. The
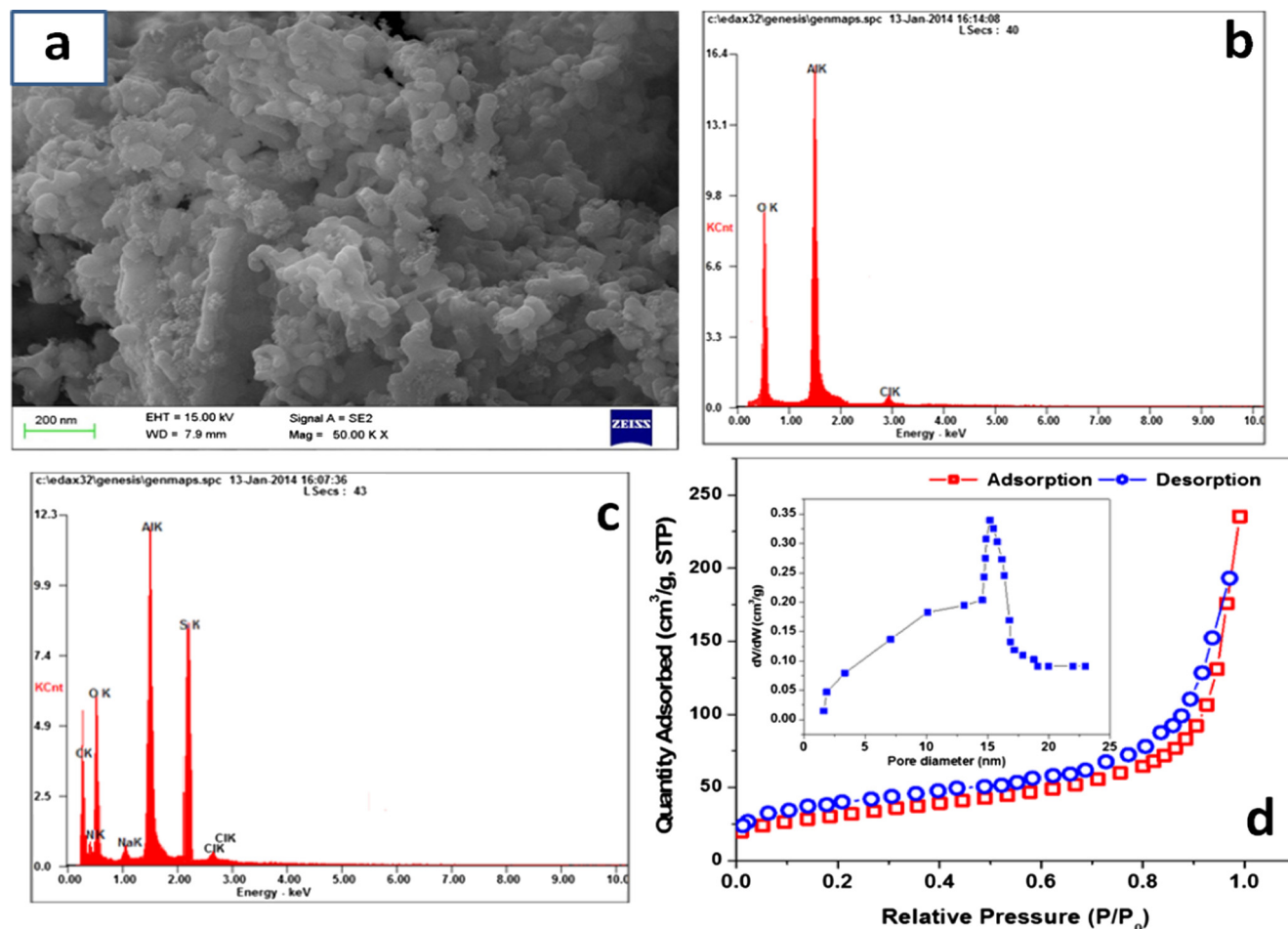

Figure 2 a: SEM micrograph of alumina nanoparticles at magnification of 50 KX; b: EDX spectra of fresh nano alumina; c: EDX spectra of dye loaded adsorbent; d: N$_2$ adsorption-desorption isotherm for alumina nanoparticles (Inset: Pore size distribution curves).

TEM image of the as-synthesized material is depicted in Fig. 1d. It is obvious from the figure that alumina particles were found to be in somewhat agglomerated state; further, the image also depicted that the particle sizes were in nanorange. The particle size distribution analysis was also investigated through TEM technique and the obtained results (Fig. 1e) suggested that most of the particles size lie within the range of 30–40 nm.

The surface morphology of the alumina nanoparticles was investigated through SEM as shown in Fig. 2a. The SEM micrograph also verified that the particle size existed in the nanoscale range. The particles were found to be clumped together as a result of the formation of a weak van der Waal bond between the particles. The particles appear to be smooth and spindle shaped. The EDX spectrum in Fig. 2b clearly shows the peak of Al and O as major constituents which confirms the formation of alumina nanoparticles. The presence of the C peaks may be due to use of carbon coating during the SEM analysis. The EDX of the sample after dye adsorption (Fig. 2c) has also been investigated. The spectra reveal the presence of relevant ions such as sulfur, nitrogen and sodium ions of the dye molecules. This provides direct evidence for the sorption of dye ions onto alumina nanoparticles.

The N_2 sorption experiments were employed for the assessment of textural properties of the sample. Fig. 2d exhibits typical type IV isotherm with an apparent hysteresis loop of type H1, which suggested that adsorbent comprises of mesoporous structures (He et al., 2015). The specific surface area was estimated by the Brunauer-Emmett-Teller (BET) equation (Barret et al., 1951) and was found to be 128 m^2/g. The estimated specific surface area was found to be larger than 125 m^2/g, which reaffirms the formation of thermodynamically stable γ-phase alumina (Zhou et al., 2007). The pore sizes were also determined by analysis of the BJH pore size distribution curves. It is clearly visible from Fig. 2d (inset) that most of the pores (approximately 90%) were lying in mesoporous range (2–50 nm diameters) and rest of the 10% were found to be in the microporous range (< 2 nm). The adsorbent average pore size and pore volume were estimated to be 13.6 nm and 0.32 cm^3/g respectively. Thus, the presence of mesoporous structures and high pore volume offers a favorable condition for the liquid phase adsorptive removal of dye ions.

The pH of zero point charge (pH_{ZPC}) of the alumina nanoparticles was determined from the point of intersection of the $pH_{initial}$ vs pH_{final} curve. pH_{ZPC} indicates the electrical neutrality of the adsorbent at certain pH values when the concentration of positively charged surface groups is the same as that of negatively charged ones. The pH_{ZPC} of alumina nanoparticles was found to be 7.4 (fig not shown) which is close to that reported by Li et al. (2011).

3.2. Effect of pH

The pH of solution is key parameter as it controls the sorption process by influencing the surface charge of adsorbent as well as adsorbate (Banerjee et al., 2014). Therefore for dye adsorption, the surface charge of the adsorbent and the dissociated forms of dyes in the solution pH is considered as a vital factor. The effect of solution pH on removal of OG by alumina nanoparticles was investigated by varying the solution pH from 2.5 to 9.5 and the results are given in Fig. 3. However, prior to analyzing the effect of pH on the absorbance of aqueous solutions of OG, pH absorbance tests were performed to make sure that changing the pH condition would have no effect on the dye absorbance characteristics. It was found that over pH range 2.5–9.5, the λ_{max} (480 nm) of the dye remains unaltered. However, between pH 10.0 and 11.5 there was a marked decrease in absorbance due to dissociation of the hydroxyl on the β-naphthol ring. Likewise studies at pH > 2.5 were not selected for experimental purposes as the pK_a value of the OG lies between 1 and 2 (Bird, 2012) which means the dye is available only in the completely ionized form beyond this value and exists as an anionic species for possible interaction with oppositely charged sites on the adsorbent. Thus, the experiments were carried out in this specified pH range and the removal of OG observed was solely due to adsorption not due to hydrolysis or chemical degradation of the dye structure. According to Fig. 3, it can be clearly seen at all initial dye concentrations that maximum removal takes place at pH 2.5, with the highest removal of 96.8% being achieved with an initial dye concentration of 50 mg/L. However, the removal percentage declined considerably with increasing pH, and minimum removal of 40.2% was recorded at pH 9.5 for a dye concentration of 125 mg/L. The removal mechanism may be elucidated on the basis of the surface chemistry of the alumina nanoparticles as it has been reported that the presence of a metal oxide in the aqueous phase results in the hydroxylation of the metal oxide surface (Wawrzkiewicz et al., 2015). Thus, metal oxide surfaces behave amphoterically and can undergo acid-base reactions in response to variable pH condition. Accordingly the probable mechanism that may be taking place is as follows:
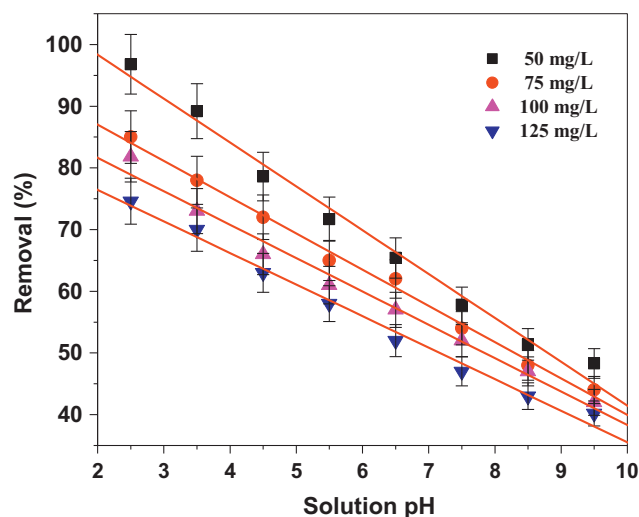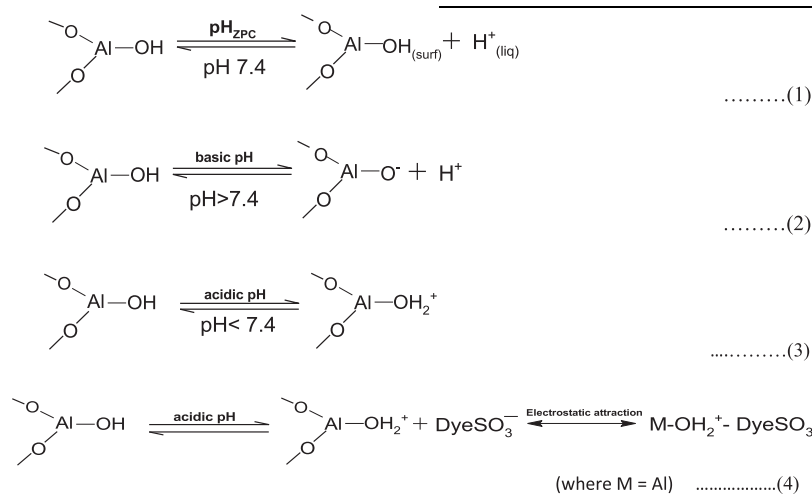

Figure 3 Effect of pH on the adsorption of Orange G on alumina nanoparticles (Temperature = 303 K; Adsorbent dose = 1.0 g/L).

$$\diagdown O\diagup Al-OH \underset{pH\ 7.4}{\overset{pH_{ZPC}}{\rightleftharpoons}} \diagdown O\diagup Al-OH_{(surf)} + H^+_{(liq)}$$

………(1)

$$\diagdown O\diagup Al-OH \underset{pH>7.4}{\overset{basic\ pH}{\rightleftharpoons}} \diagdown O\diagup Al-O^- + H^+$$

………(2)

$$\diagdown O\diagup Al-OH \underset{pH<7.4}{\overset{acidic\ pH}{\rightleftharpoons}} \diagdown O\diagup Al-OH_2^+$$

…..………(3)

$$\diagdown O\diagup Al-OH \overset{acidic\ pH}{\rightleftharpoons} \diagdown O\diagup Al-OH_2^+ + DyeSO_3^- \overset{Electrostatic\ attraction}{\rightleftharpoons} M-OH_2^+-DyeSO_3^-$$

(where M = Al)   ………………(4)

The above reactions suggest that the surface properties of alumina nanoparticles are strongly governed by the aqueous pH condition. Reaction (1) suggests that at a pH 7.4, the net surface charge of the adsorbent is zero and it becomes electrically neutral. Conceptually at pH > pH_{ZPC} in basic medium (reaction (2)), the adsorbent surface becomes negatively charged due to deprotonation; thus, the adsorption of anionic dye ions gets severely hindered as a result of columbic repulsion. In acidic pH condition (reaction (3)), when the pH < pH_{ZPC} the surface is charged positively and this electrostatically attracted the anionic OG species and leads to a higher adsorption of dye anions (reaction (4)). Hence, a pH of 2.5 was taken as the optimum pH for which the adsorbent efficiency for the removal of dye is a maximum. A similar observation has been reported by Zheng et al. (2012) and Monash and Pugazhenthi (2014) for the adsorption of the anionic dye, Methyl orange.

3.3. Effect of co-existing ions

It is well known that wastewater discharged from the textile industries is often contaminated with inorganic anions which impede the adsorption process. For this reason, the effect of inorganic anions on adsorption capacity of OG ions was investigated. Fig. 4 shows the effect of the coexisting ions for different inorganic anions, including NO_3^-, Cl^-, CO_3^{2-}, SO_4^{2-}, PO_4^{3-} and $C_2O_4^{2-}$, have been selected as the competitive ions in the adsorption experiments. It has been observed that the adsorption of OG in the presence of NO_3^-, Cl^- and CO_3^{2-} ions was not affected significantly. However SO_4^{2-}, PO_4^{3-} and $C_2O_4^{2-}$ anions exhibit a remarkable effect on the adsorption performance of OG. With the slight increase in concentration of PO_4^{3-} and $C_2O_4^{2-}$ ions, the adsorption efficiency of OG plunges down below 30 mg/g. For the case of SO_4^{2-} the adsorption efficiency seems to be affected appreciably at higher SO_4^{2-}, concentrations. The high affinity of alumina nanoparticles for SO_4^{2-}, PO_4^{3-} and $C_2O_4^{2-}$ ions may be attributed to formation of outer-sphere surface complexes on the surface of metal hydroxides (Hordern, 2004). Thus, the study of anions envisaged that the presence of SO_4^{2-}, PO_4^{3-} and $C_2O_4^{2-}$ ions in aqueous solution was identified as a critical limiting factor in the treatment process when alumina nanoparticles were employed as adsorbent.

3.4. Effect of contact time and sorption kinetics

The effect of contact time on OG sorption by alumina particles was studied at 303 K and results are shown in Fig. 5. It was observed that the extent of sorption increased with the increase in contact time up to 30 min and then the sorption attained equilibrium. This suggested that the time required for OG-alumina nanoparticles interactions to attain steady state was just 30 min for all initial dye concentrations which further implies that the interaction is independent of initial OG concentrations. Therefore, all experiments were conducted for 30 min. The rapid removal in the initial stages (> 50% removal accounted for all dye concentrations within 5 min) may be due to the fact that initially all the sorption sites were vacant and could adsorb more dye anions from the solution phase (Ghaedi et al., 2012). As the sorption process advanced, the adsorption rate decreased steadily owing to incursion of OG ions deep into the pores of the adsorbent and finally the adsorption curves maintained a flattening profile indicating almost complete saturation of the sorption sites.
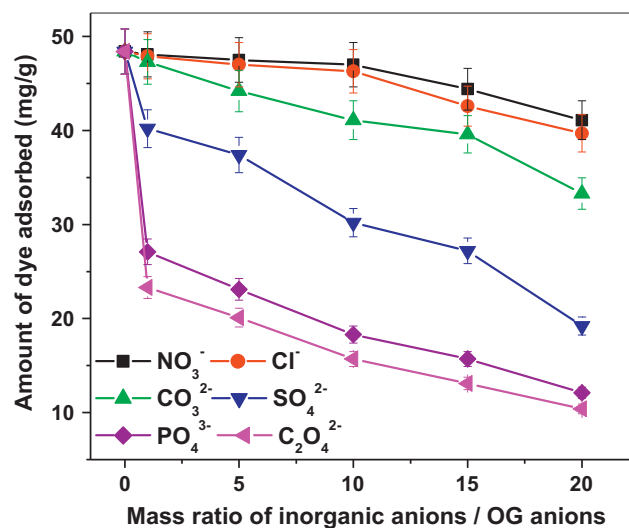

Figure 4 Effect of dye uptake in the presence of coexisting anions (dye concentration 50 mg/L; temperature 303 K; dose 1.0 g/L; pH 2.5).
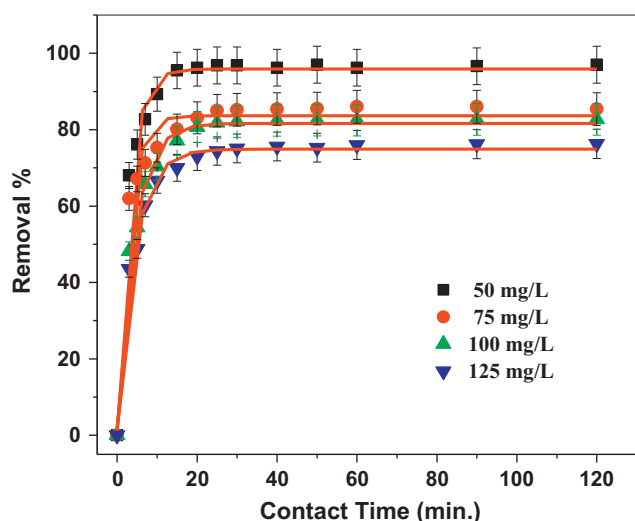
Figure 5 Effect of contact time for adsorption of Orange G on alumina nanoparticles for different initial dye concentrations (pH 2.5, adsorbent dose 1.0 g/L, temperature 303 K).

Investigation of sorption kinetics helps in elucidating the mechanism that controls the sorption process. As it is quite certain, process variables play an imperative role in adsorption processes by influencing the physicochemical nature of the adsorbate-adsorbent and consequently control the removal rate. Therefore, interpretation of sorption kinetics data in terms of different process parameters including pH, temperature and initial dye concentration will provide valuable insights about the sorption mechanism. In the present study, kinetic data were analyzed by fitting them into two important kinetic models, namely the pseudo-first order (Lagergren, 1898) and the pseudo-second order (Ho and McKay, 1999).

The linearized form of the pseudo-first order equation is (Ho and McKay, 1999):

$$\log(q_e - q_t) = \log q_e - (k_1/2.303) \cdot t \quad (5)$$

where q_t and q_e represent the amount of dye adsorbed (mg/g) at any time t and at equilibrium time, respectively, and k_1

represents the adsorption rate constant (min^{-1}). The sorption kinetic data obtained experimentally for each process variable were fitted as a plot of 'log $(q_e - q_t)$ vs t' (Figure not shown). The resultant plots were found to obey the first order kinetics only for an initial adsorption period of 15 min beyond that the plots become nonlinear. Moreover, the correlation coefficient values for the pseudo-first order are very low and the predicted q_e values diverge significantly from the experimental q_e values which further indicated the inadequacy of the first-order kinetic model to correctly predict the kinetics of OG sorption. The ineptness of this model directed us to investigate the adsorption processes of OG by applying pseudo-second-order kinetic model to fit the experimental data. The parameters calculated for first order kinetics were provided in Table 1.

The pseudo-second order model in linearized form is given as (Ho and McKay, 1999):

$$t/q_t = 1/k_2 \; q_e^2 + t/q_e \quad (6)$$

where k_2 (g/mg min), is the second order rate constant which can be calculated from the intercept of the graph plotted between t/q_t versus t, and q_e values have been evaluated from the slope of same graph and represented in Table 1. The pseudo second order kinetic plots are given in Fig. 6a–c. The kinetic plots obtained for the various parameters yielded a linear relationship over the entire period of time; moreover, the values of q_e calculated from the second order plots are in good agreement with the experimental values of q_e with small deviations and higher R^2 values ($R^2 > 0.995$) suggested that the OG sorption system follows second-order kinetics.

Meanwhile, on inspection of the first and second order rate constants (Table 1), a decreasing trend has been noticed with an increase of pH and temperature while the rate constant follows a rising trend with increasing initial dye concentration. The trend observed for pH values may be due to a reluctance of the dye anions to diffuse across the barrier layer when negatively charged hydroxyl groups dominate, and similarly with the increase in solution temperature, rate constant values decline which may be attributed to the poor interaction between dye ions and active sites on the adsorbent due to the weakening of physical forces. This further interrupted effective mass transfer of dye ions from bulk to solid surface.

Table 1 Kinetics parameters for the adsorption of OG by alumina nanoparticles.

| Process variables		Pseudo-first order			Pseudo-second order			Intra-particle diffusion					
	$q_{e,exp}$	k_1 min^{-1}	$q_{e,cal}$ mg/g	R^2	k_2 g mg^{-1} min	$q_{e,cal}$ mg/g	R^2	$k_{id,1}$ mg^{-1} g min$^{0.5}$	C_1 (mg/g)	R^2	$k_{id,2}$ mg^{-1} g. min$^{0.5}$	C_2 (mg/g)	R^2
Solution pH (Experimental condition: Temperature 303 K; Dye conc. 50 mg/L)													
2.5	48.5	0.13	26.5	0.972	0.0023	50.1	0.999	8.44	18.27	0.974	1.12	46.14	0.982
4.5	39.3	0.09	19.2	0.976	0.0011	41.4	0.999	7.97	9.77	0.982	1.04	29.33	0.954
8.5	26.7	0.04	15.8	0.983	0.0006	29.2	0.999	5.62	4.43	0.986	0.97	21.64	0.944
Adsorption temperature (Experimental condition: pH 2.5, Dye conc. 50 mg/L)													
303 K	48.5	0.13	26.5	0.972	0.0023	50.1	0.999	8.44	18.27	0.974	1.12	46.14	0.982
313 K	43.6	0.11	24.7	0.982	0.0016	46.1	0.999	6.36	10.43	0.985	1.26	37.30	0.937
323 K	38.8	0.07	20.6	0.981	0.0013	41.6	0.999	4.42	8.11	0.982	0.33	34.44	0.978
Initial dye concentration (Experimental condition: pH 2.5, temperature 303 K)													
75 mg/L	63.4	0.15	51.2	0.966	0.0044	66.1	0.999	11.92	36.19	0.991	2.16	51.94	0.969
100 mg/L	81.8	0.18	72.4	0.987	0.0049	83.4	0.999	14.69	24.40	0.964	2.84	66.83	0.916
125 mg/L	87.5	0.21	77.4	0.988	0.0067	90.1	0.999	15.34	26.62	0.977	3.03	71.31	0.978
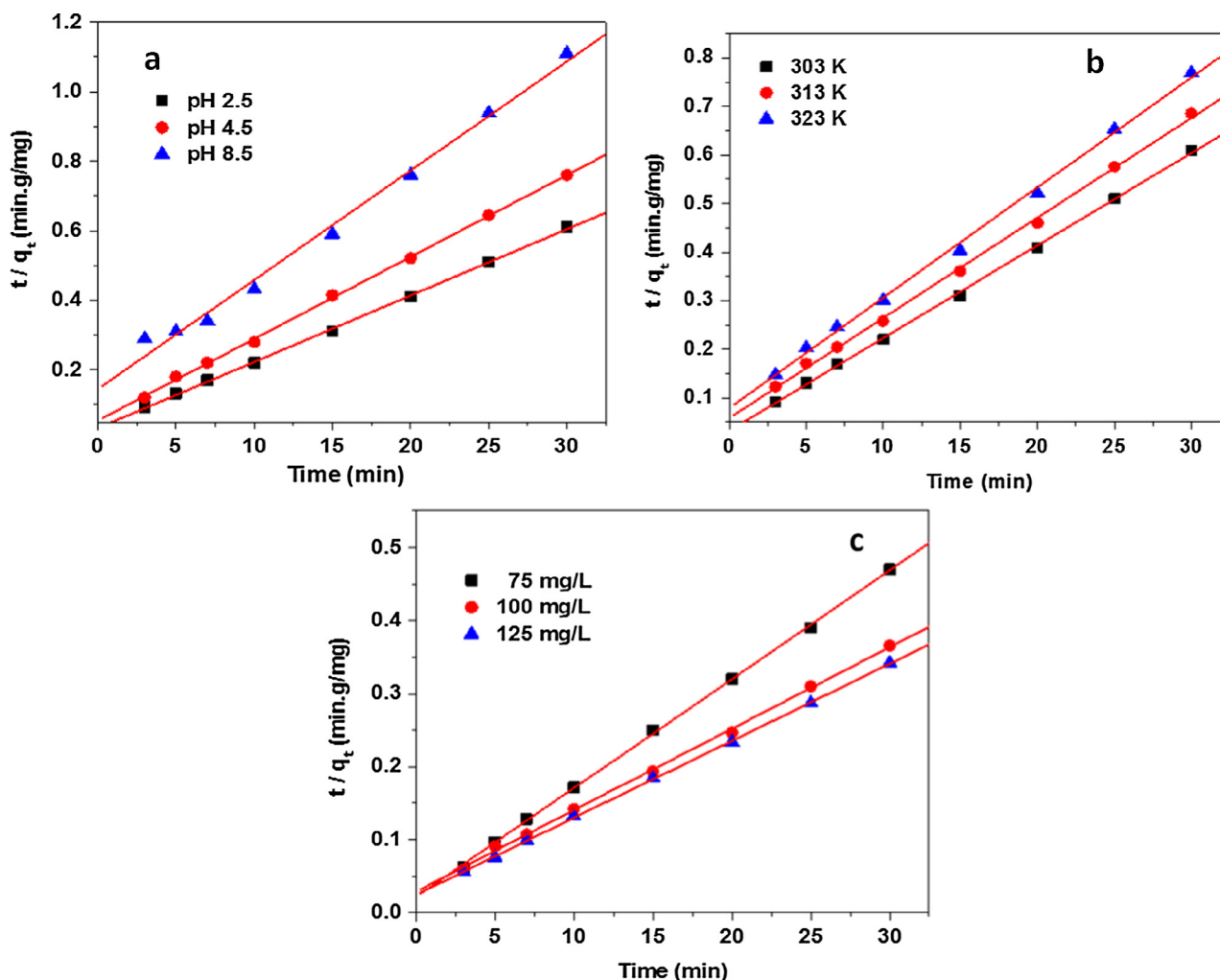
Figure 6   Pseudo-second order kinetic plots obtained for various process parameters.

In case of initial dye concentration, the rate constant values increased with dye concentrations which might have occurred due to the enhanced concentration gradient that easily surmounts the mass transfer resistance experienced by dye ions (Allen et al., 2005).

3.5. Adsorption mechanism

The actual mechanistic step that controls the overall rate of the sorption process can be investigated by employing the kinetic data into well-known mathematical models i.e. intraparticle diffusion model recommended by Weber and Morris (1963). Theoretically, plots with a linear relationship and a zero intercept are the requisite aspect that determines this model's suitability as well as indicative of pore diffusion as a rate controlling step. The intraparticle diffusion model is given as follows (Weber and Morris, 1963):

$$q_t = k_{id} t^{1/2} + C \tag{7}$$

where parameter k_{id} (mg/g min$^{0.5}$) is the rate constant for intraparticle diffusion and C (mg/g) is the intercept and is an indicator of the boundary layer thickness. Fig. 7a–c, represents the intra-particle diffusion plots obtained for various process parameters. It is clear from these figures that that plots of 'q_t versus $t^{0.5}$' are not straight over the entire time range and are 'found to be segregated into two linear sections. The multi segmented plots validate the participation of multiple phenomena during adsorption of OG by alumina nanoparticles. The first linear plot demonstrates external mass transfer, in which the adsorbate migrated through solution to the external surface of the adsorbent resulting in high uptake rate; afterward, the solute molecules make their way into the interior of the adsorbent through intra-particle diffusion, as illustrated by the second linear plot. The results suggest that intraparticle diffusion is not the sole rate limiting step and the present sorption process is jointly controlled by film diffusion and an intra particle diffusion mechanism. Moreover, the rate constant (k_{id}) values calculated for the intraparticle diffusion model (Table 1) follow the comparable trend as that reported for pseudo-first order and pseudo-second order kinetics.

It has already been confirmed from the intra-particle diffusion study that more than one mechanisms seem to control the sorption process, but the model fails to express the precise rate determining step. This setback can be overcome by treating experimental kinetic data further with the external diffusion model and internal diffusion model (Piccin et al., 2011). The external mass transfer model assumes that the concentration
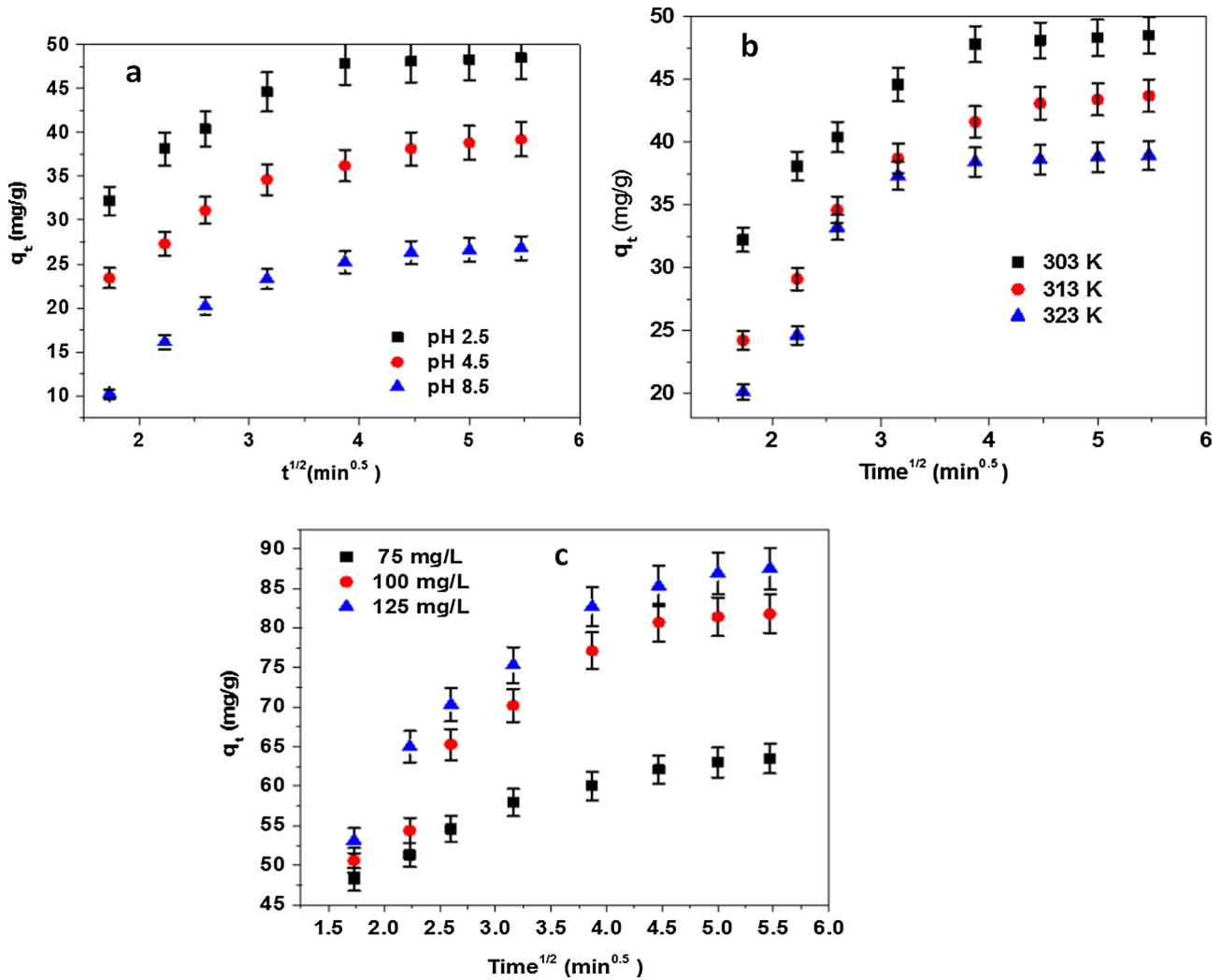
Figure 7 Intra-particle diffusion plots obtained for various process parameters.

at the solid surface approaches to zero and the intraparticle diffusion is negligible during initial period of contact time. External mass transfer has been represented as follows (Piccin et al., 2011):

$$\frac{q_t}{q_e} = \frac{C_i}{C_i - C_e}\left[1 - \exp\left\{-k_f \frac{A}{V} t\right\}\right] \quad (8)$$

where q_t and q_e refer to the amount of OG adsorbed (mg/g) at any time, t (min), and at equilibrium respectively, C_i and C_e are the initial and equilibrium concentrations of the adsorbate in aqueous solutions, respectively, k_f is the external mass transfer coefficient (m/min) and A/V is the volumetric area of the particle (m^{-1}). The k_f values obtained from the fit of Eq. (7) have been provided in Table 2.

A reliable estimate of the diffusivities for film diffusion and pore diffusion model can be evaluated using models proposed based on Fickian diffusion principle given as (Crank 1975):

$$\frac{q_t}{q_e} = 6\sqrt{\left(D_{film}/\pi r_p^2\right)} \cdot \sqrt{t} \quad (9)$$

$$\frac{q_t}{q_e} = 1 - \exp\left[\ln\left(\frac{6}{\pi^2}\right) - \left(\frac{D_{pore}\pi^2}{r_p^2} \cdot t\right)\right] \quad (10)$$

where D_{film} and D_{pore}, refer to external and internal diffusivity coefficients (m^2/min) and r_p is the radius of the alumina nanoparticles (m).

Thus, the model film diffusivity and pore diffusivity have been fitted with the experimental data acquired from the corresponding first linear plot and second linear plot, respectively from the Weber-Morris model. The parameters D_{film}, and D_{pore} were evaluated from the plot based on Eqs. (9) and (10) and values are presented in Table 2.

Now, the parameters including k_f and D_{pore}, that have already been evaluated from their respective models have been further employed for the determination of a dimensionless parameter named as Biot number (Bi_N). This parameter facilitates determination of the rate limiting step of the sorption process. The parameter basically relates external mass transfer coefficient to the diffusion coefficient (Dizge et al., 2008). Thus, the influence of various parameters on the dye adsorption resistance can be examined through the Biot number given by the following expression (Dizge et al., 2008):

$$Bi_N = k_f r C_i / \rho_a D_{pore} q_0 \quad (11)$$

where k_f is external mass transfer coefficient (m/min), r is radius of the adsorbent particle (m), q_0 is the adsorption capacity (mg/g) assuming $C_e = C_0$. ρ_a is the adsorbent particle

Table 2 Mass transfer, film and pore diffusion coefficients and Biot number calculated for the adsorption of OG by alumina nanoparticles.

Process variables	K_L (m/min)	D_{film} (m^2/min)	D_{pore} (m^2/min)	Bi_N
pH (Experimental condition: Temperature = 303 K; Adsorbent dose = 1.0 g/L; Dye concentration = 50 mg/L; Average particle size = 32 nm; Adsorbent density 3870 kg/m^3)				
2.5	2.46×10^{-7}	3.61×10^{-8}	5.54×10^{-17}	1.8×10^{-2}
4.5	1.33×10^{-7}	3.27×10^{-8}	4.02×10^{-17}	2.1×10^{-2}
8.5	7.76×10^{-8}	2.92×10^{-8}	2.67×10^{-17}	2.8×10^{-2}
Temperature (Experimental condition: pH = 2.5; Adsorbent dose = 1.0 g/L; Dye concentration = 50 mg/L; Average particle size = 32 nm; Adsorbent density 3870 kg/m^3)				
303 K	2.46×10^{-7}	3.61×10^{-8}	5.54×10^{-17}	1.8×10^{-2}
313 K	2.12×10^{-7}	2.35×10^{-8}	5.07×10^{-17}	2.7×10^{-2}
323 K	1.77×10^{-7}	2.11×10^{-8}	3.03×10^{-17}	3.5×10^{-2}
Initial dye concentration (Experimental condition: pH = 2.5; Temperature = 303 K; Adsorbent dose = 1.0 g/L; Average particle size = 32 nm; Adsorbent density 3870 kg/m^3)				
75 mg/L	2.92×10^{-7}	5.12×10^{-8}	6.72×10^{-17}	2.2×10^{-2}
100 mg/L	3.07×10^{-7}	6.66×10^{-8}	7.43×10^{-17}	1.9×10^{-2}
125 mg/L	4.38×10^{-7}	9.37×10^{-8}	9.80×10^{-17}	1.4×10^{-2}

density (kg/m^3), and D_{pore} is internal pore diffusion coefficients (m^2/min). The calculated values of Bi_N are given in Table 2.

It can be seen from Table 2 that with the increase of pH and temperature, the resistance to the mass transfer increased and likewise, film diffusion and pore diffusion values were found to follow a retarding trend. However, opposite trend can be noticed for the Biot number which indicates an increase of resistance in the diffusion mechanism causing delay in the sorption process. In the case of initial dye concentration, the decrease in the resistance to mass transfer with the increase in dye concentration has been identified by the increase of the k_f values. This behavior is attributed to the effective driving force assisted to overcome the mass transfer resistance of the dye ions between liquid and solid phases. Meanwhile, the diffusion coefficients also exhibited a rising trend but the Bi_N values noticeably decline with dye concentration. Thus, high k_f and D_{film} values indicate that the external diffusion mechanism is significant on control of the sorption process which is further substantiated by a decrease in the Biot number with an increase in the dye concentrations. Moreover, as suggested by Dizge et al. (2008), the Biot number is a decisive factor that helps in deciding the predominance of surface diffusion against external diffusion, in case where the Biot number >100 adsorption processes are considered to be controlled by internal diffusion mechanisms. Cooney (1993) and Dotto et al. (2014), recommend that for Bi_N < 0.5, a complete dominance of the external mass transfer resistance can be anticipated while for Bi_N > 10, a considerable dominance of the intraparticle resistance is possibly expected. Thus, on the basis of above hypothesis, in the present sorption system, the as-evaluated Bi_N values indicate that external mass transfer predominantly controls the sorption of OG anions on alumina nanoparticles.

3.6. Adsorption isotherm

The isotherm study helps in interpreting the interaction between the dye concentration in aqueous phase and the amount of dye adsorbed per unit weight of adsorbent at constant temperature. The study was performed by employing the well-known isotherm models viz. Langmuir (1918), Freundlich

(1906), and Dubinin-Radushkevich (1947), to the present system at different temperatures. It has been observed that for all temperatures, the sorption capacity for OG anions by alumina nanoparticles enhanced steadily with increase in initial dye concentration and ultimately approached saturation phase at higher dye concentration (Fig. 8). The adsorption capacity at equilibrium increased from 48.4 to 84.4 mg/g with the increase in initial OG concentrations from 50 to 125 mg/L. The increase in uptake capacity with concentration was anticipated as a result of high driving force for mass transfer (Banerjee et al., 2015).

For the isotherm investigations, the experimental data are correlated by the isotherm expressions given as follows:

Langmuir model in linearized form:

$$1/q_e = 1/q_{max} + 1/C_e b q_{max} \tag{12}$$

Freundlich model in linearized form:

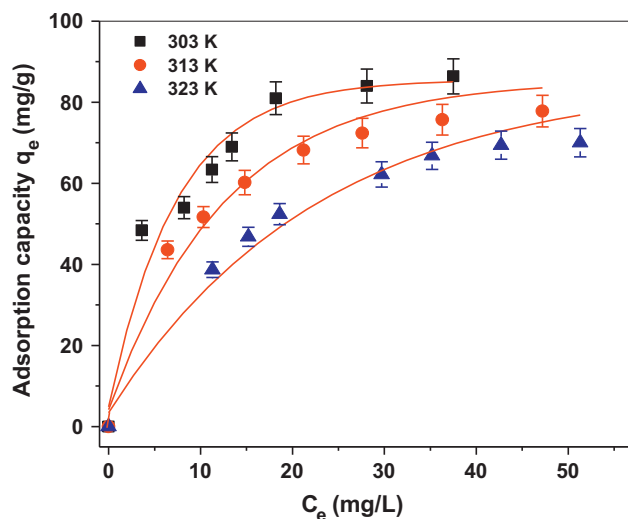$$\log q_e = \log K_F + 1/n \log C_e \tag{13}$$

Figure 8 Isotherm plots for adsorption of Orange G on alumina nanoparticles at different temperatures.

D-R model in linearized form:

$$\ln q_e = \ln q_m - \beta\varepsilon^2 \tag{14}$$

$$E = 1/(2\beta)^{0.5} \tag{15}$$

where C_e (mg/L) and q_e (mg/g) are the concentrations of adsorbate and amount of adsorbate adsorbed at equilibrium, respectively. The constant b (L/mg) is the Langmuir equilibrium constant and q_{max} gives the theoretical monolayer saturation capacity. K_F (mg/g) is the Freundlich constant and n is the Freundlich exponent. The constant K_F is related to the degree of adsorption, $1/n$ gives the tentative estimation of the intensity of the adsorption, q_m is the theoretical monolayer saturation capacity (mg/g), β is the D-R model constant (mol^2/kJ^2), and ε is the Polanyi potential.

The calculated values of the adsorption isotherm parameters and error functions for OG sorption onto alumina nanoparticles are listed in Table 3. As the error function and R^2 values determine the applicability of the isotherm model, according to the results, high R^2 values and low HYBRID values obtained for the Langmuir isotherm model indicated suitability of this model in expressing equilibrium sorption data. Furthermore, the suitability of the model indicates that dye is adsorbed as a monolayer onto a sorbent surface having a finite number of identical sorption sites. Meanwhile, the parameters calculated for D-R model help in predicting the nature of sorption process and possibility of adsorbent regeneration. The value of E can be evaluated from Eq. (15). If the values lie in between 8 and 16 kJ/mol, the adsorption process is supposed to be controlled by a chemisorption mechanism, while the values of E less than 8 kJ/mol indicate involvement of physical adsorption (Banerjee et al., 2015). Thus the estimated E values were found to be < 8 kJ/mol which suggests that physical forces might be responsible for the interaction between OG anions and alumina nanoparticles. As the physisorption process is known to be reversible in nature (Dabrowski, 2001), this further recommends that the exhausted adsorbent can be easily regenerated via desorption.

3.7. Thermodynamic investigation

The thermodynamic behavior of the sorption process was investigated by estimating the thermodynamic parameters viz. change in free energy, enthalpy and entropy using the following well-known equations (Uma et al., 2013; Gautam et al., 2015):

$$\Delta G = -RT \ln K_c \tag{16}$$

$$\ln K_c = \Delta S°/R - \Delta H°/RT \tag{17}$$

where K_c can be calculated using relationship q_e/C_e, R is the ideal gas constant (kJ/mol/K) and T is the temperature (K). The enthalpy change ($\Delta H°$) and the entropy change ($\Delta S°$) are calculated from a plot of $\ln K_c$ versus $1/T$ (fig. not shown). The values estimated for Gibbs free energy at 303, 313 and 323 K were -8.5, -4.9 and -4.2 kJ/mol respectively, indicating that the adsorption process is spontaneous in nature; besides, the decrease in negative values of $\Delta G°$ with increasing temperature implies that adsorption was favorable at low temperature. The values obtained for $\Delta G°$ can also be used to differentiate between physical and chemical adsorption. The former case is valid when $\Delta G°$ values estimated are between -20 and 0 kJ/mol, and the later is between -80 and -400 kJ/mol (Banerjee et al., 2014). Thus the calculated $\Delta G°$ values indicated about the involvement of physisorption. Likewise, the negative value of $\Delta H°$ (-19.4 kJ/mol) confirms the exothermic nature of the sorption process and this observation has been in accordance with the OG adsorption capacities which decreased with increasing adsorption temperature. The $\Delta H°$ values were found to be in 2–21 kJ/mol range which indicated that physical forces dominate the sorption mechanism. The negative value of $\Delta S°$ (-248 J/mol K) recommends that adsorbate concentration increases on solid adsorbent surface that leads to a decrease in randomness at solid-liquid interface decreased during adsorption of OG anions.

3.8. Regeneration of adsorbent

Regeneration of adsorbent for repeated reuse is highly desirable and this not only makes the treatment process economically viable but also offers a prospective solution for the management of contaminant loaded adsorbent. In the present work, in order to determine the effectiveness of different solutions toward desorption, desorbing solutions such as 0.1 M HCl, 0.1 M HClO$_4$, 0.1 M HNO$_3$, 0.1 M H$_2$SO$_4$, and 0.1 M H$_3$PO$_4$ were tested. The study was conducted in batch mode using 1 g/L of dye loaded sorbent in 100 mL of desorbing solution and the contents agitated in a water bath shaker at 303 K until equilibrium was achieved. The solution was analyzed spectrophotometrically for the determination of desorbed dye concentration. Desorption results have been illustrated in increasing manner as H$_3$PO$_4$ 83% < H$_2$SO$_4$ 87% = HNO$_3$ 87% < HCl 91% < HClO$_4$ 93% (Fig. 9). The desorption trend further indicated that ion exchange mechanism governed the desorption process. Thus, with significant desorption potential, HClO$_4$ was selected for the regeneration and reusability study. It has been investigated that after four cycles of the adsorption-desorption process, the dye removal percentage was still more than 67% after which the removal of OG declined drastically. Thus, the study clearly demonstrated that
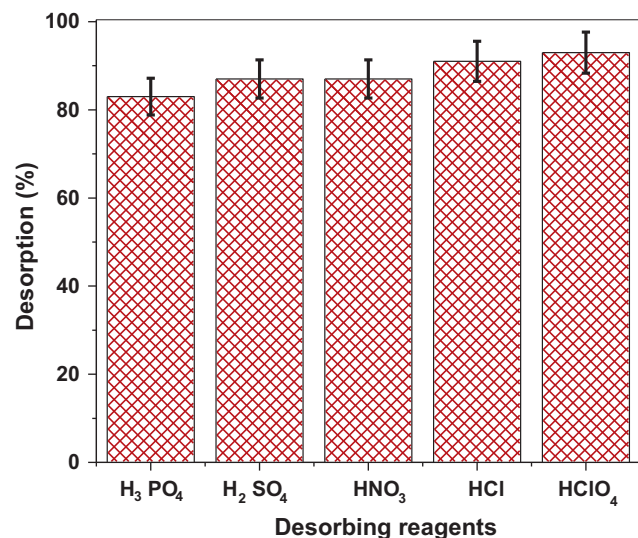
Table 3 Various equilibrium isotherm coefficients obtained for sorption of OG on alumina nanoparticles.

Dye	Model	303 K	313 K	323 K
Orange G	**Langmuir**			
	Q_{max} (mg/g)	93.3	88.9	82.5
	b (L/mg)	0.33	0.16	0.09
	R^2	0.999	0.995	0.996
	HYBRID	19.4	27.1	23.6
	Freundlich			
	K_F (mg/g)(L/mg)$^{1/n}$	4.28	2.65	1.56
	n	5.26	3.57	2.44
	R^2	0.971	0.978	0.965
	HYBRID	46.3	33.8	41.8
	Dubinin-Radushkevich			
	q_m (mg/g)	62.4	57.7	52.2
	β (mol^2/kJ^2)	0.04	0.07	0.09
	E (kJ/mol)	3.57	2.67	2.35
	R^2	0.975	0.899	0.904
	HYBRID	58.4	63.7	52.1

Figure 9 Regeneration of alumina nanoparticles using different desorbing reagents.

alumina nanoparticles can be efficiently reused up to four cycles for the removal of OG from aqueous solutions without much loss of removal capacity.

3.9. Stability of adsorbent

As it is a well-known fact that solution pH influences the mobility of metal ions, possibility of leaching of aluminum ions from alumina nanoparticles into treated water can be anticipated when the same was employed for water treatment. Therefore, it is desirable to investigate the stability of the

synthesized alumina nanoparticles by performing a leaching test in aqueous solution at variable pH condition. The experimental results suggested that the concentration of leached aluminum ions for all pH conditions (2.5–9.5) was estimated to be not more than 0.082 ppm which further infers that alumina nanoparticles exhibited reasonable stability in various aqueous media and can be safely used for treatment of the wastewater.

3.10. Assessment of sorption behavior of alumina nanoparticles using real wastewater

For this study, dye contaminated real wastewater was procured from the carpet industry located near Varanasi

Table 4 Physicochemical analysis of carpet industry wastewater.

Parameter	Characteristics
Color	Reddish brown
pH	7.6
Dissolved solids (mg/L)	13,100
Suspended solids (mg/L)	900
Total solids (mg/L)	14,000
Biochemical oxygen demand (mg/L)	327
Chemical oxygen demand (mg/L)	931

(Bhadohi, Uttar Pradesh, India). As the study comprised of model dye Orange G, therefore, wastewater sample was collected particularly from that industry only where OG was used. Moreover, during dyeing operations, other dyes were also used. In present investigations, it has been examined that along with Orange G two other dyes namely Indigo carmine and Reactive red 180 were also present in the sample and all these dyes were chemically anionic in nature. The effluent was then analyzed for various physicochemical parameters as depicted in Table 4. The BOD_5 measurement was carried out by BOD incubator (Adair Dutt & Company Pvt. Ltd., New Delhi) and for COD analysis was carried out by digestion apparatus (Mac Scientific Equipment, New Delhi). The results of the sampled wastewater analysis revealed that as expected, the wastewater contained high BOD_5 and COD. The concentration of the dyes present in the water sample was measured spectrophotometrically, the measurement for ternary dye system (OG + IC + RR180) has been carried out at their maximum absorbance wavelength $\lambda_{1,max}$ (480 nm), $\lambda_{2,max}$ (608 nm) and $\lambda_{3,max}$ (543 nm) respectively, and absorbance was recorded as A_1, A_2 and A_3. The concentrations of specific dye forms were estimated using equa***tion given as follows:

$$C_A = \frac{A_1 k_{B3} k_{C2} - A_1 k_{B2} k_{C3} + A_2 k_{B1} k_{C3} - A_2 k_{B3} k_{C1} + A_3 k_{B2} k_{C1} - A_3 k_{B1} k_{C2}}{k_{A1} k_{B3} k_{C2} - k_{A1} k_{B2} k_{C3} + k_{A2} k_{B1} k_{C3} - k_{A2} k_{B3} k_{C1} + k_{A3} k_{B2} k_{C1} - k_{A3} k_{B1} k_{C2}} \quad (18)$$

$$C_B = \frac{A_1 k_{A2} k_{C3} - A_1 k_{A3} k_{C2} + A_2 k_{A3} k_{C1} - A_2 k_{A1} k_{C3} + A_3 k_{A1} k_{C2} - A_3 k_{A2} k_{C1}}{k_{B1} k_{A2} k_{C3} - k_{B1} k_{A3} k_{C2} + k_{B2} k_{A3} k_{C1} - k_{B2} k_{A1} k_{C3} + k_{B3} k_{A2} k_{C2} - k_{B3} k_{A2} k_{C1}} \quad (19)$$

$$C_C = \frac{A_1 k_{A2} k_{B3} - A_1 k_{A3} k_{B2} + A_2 k_{A3} k_{B1} - A_2 k_{A1} k_{B3} + A_3 k_{A1} k_{B2} - A_3 k_{A2} k_{B1}}{k_{C1} k_{A2} k_{B3} - k_{C1} k_{A3} k_{B2} + k_{C2} k_{A3} k_{B1} - k_{C2} k_{A1} k_{B3} + k_{C3} k_{A1} k_{B2} - k_{C3} k_{A2} k_{B1}} \quad (20)$$

where A, B, and C represent the different dye forms having wavelengths of $\lambda_{1,max}$, $\lambda_{2,max}$, and $\lambda_{3,max}$ respectively, and k_{A1}, k_{A2}, k_{A3}, k_{B1}, k_{B2}, k_{B3}, k_{C1}, k_{C2}, and k_{C3} are the various calibration constants measured for the dye forms A, B and C. The result depicting concentrations of the various dye components present in the effluent sample is given in Table 5.

Now, the most important part of the investigation was the assessment of the performance of alumina nanoparticles in a multi-solute system. The study is found to be very important from the industrial viewpoint as the dyeing effluents comprised of mixed solute system; therefore, the results of the adsorption experiments performed using single solute system may vary from those of multi-solute system. Therefore, it is desirable

Table 5 Industrial effluent from carpet industry before and after adsorption with alumina nanoparticles.

Dyes present in the wastewater	Orange G	Indigo carmine	Reactive red 180	BOD of the effluent after treatment (mg/L)	COD of the effluent after treatment (mg/L)
Concentration determined in wastewater (mg/L)	19.4	17.3	24		
Amount adsorbed (mg/g) at pH 7.6	5.2 (26.8%)	4.1 (23.6%)	5.7 (23.7%)	213 (34.8%)	557 (40.2%)
Amount adsorbed (mg/g) at pH 2.5	12.4 (63.9%)	11.1 (64.1%)	13.6 (56.6%)	118 (63.9 %)	307 (67.1%)

to compare the removal efficiency of alumina nanoparticles for simulated and real wastewater. Batch adsorption experiments were carried out using 100 mL of sample (real wastewater) with adsorbent dose of 1.0 g/L at constant temperature of 303 K and at pH 7.6 and 2.5, respectively. The results (Table 5) imply that treatment of effluents without making any pH adjustment resulted in insignificant adsorption of dye effluents; however, when the pH of the effluents is adjusted to 2.5, an enhanced sorption performance can be observed for all the dyes. Nevertheless, a pH dependent removal process follows a similar trend as that for batch studies but the amount of dye uptake reduces significantly for mixed dye systems in comparison with single solute systems. However, the results obtained for the uptake capacity appear to be significant as the removal percentages for all the dyes remain more than 50% which indicate that the adsorbent is equally effective for a multi-solute system. Furthermore it has also been investigated that the adsorbent is highly proficient in lowering the organic load such as BOD and COD from the real industrial waste effluents.

4. Conclusions

The following logical conclusions can be drawn:

- Alumina nanoparticles (γ alumina) were successfully synthesized via sol gel technique and the particle size was found to be in the range of 30–35 nm.
- FTIR spectra of bare alumina nanoparticles indicated the formation of γ-phase.
- X-Ray diffraction patterns confirm the formation of γ-phase alumina.
- The formation of nanoscale alumina particles was validated from TEM and SEM analysis.
- The data interpreted from N_2 adsorption-desorption isotherm indicated adsorbent is mesoporous with a specific surface area of 128 m^2/g.
- Solution pH plays a prominent role in dye removal process as acidic pH condition favors uptake capacity of the adsorbent, and maximum removal was achieved at pH 2.5.
- The presence of interfering anions (PO_4^{3-}, CO_3^{2-} and SO_4^{2-}) demoted dye removal performance of the adsorbent.
- Initial dye concentration and contact time were found to influence the sorption process. Removal (%) of OG was found to increase with decreasing initial dye concentration.
- The process of removal of OG by adsorption on nano alumina is governed by second order kinetics.
- The Weber-Morris and diffusion models depicted that the mechanism of removal process was controlled by both the film and pore diffusion but external diffusion controls the overall rate of the sorption process.

- The study on sorption isotherm data indicates Langmuir isotherm as the best suited model and maximum sorption capacity is evaluated as 93.3 mg/g at 303 K.
- Thermodynamic investigations indicate that the sorption of OG on alumina nanoparticles is spontaneous and exothermic in nature.
- Desorption studies demonstrated that the adsorbent can be effectively reused for at least four cycles without significant loss in sorption capacity.

Thus, the above results support the recommendation that alumina nanoparticles offer new dimensions toward reliable and economically viable water treatment of colored effluents. The material is very promising and can be effectively used and re-used for the removal of anionic dyes from the aqueous solutions.

References

Afkhami, A., Tehrani, M.S., Bagheri, H., 2010. Simultaneous removal of heavy-metal ions in wastewater samples using nano-alumina modified with 2, 4-dinitrophenylhydrazine. J. Hazard. Mater. 181, 836.

Ali, I., 2012. New generation adsorbents for water treatment. Chem. Rev. 112, 5073.

Allen, S.J., Gan, Q., Matthews, R., Johnson, P.A., 2005. Mass transfer processes in the adsorption of basic dyes by peanut hulls. Ind. Eng. Chem. Res. 44, 1942.

Banerjee, S., Gautam, R.K., Jaiswal, A., Chattopadhyaya, M.C., Sharma, Y.C., 2015. Rapid scavenging of methylene blue dye from a liquid phase by adsorption on alumina nanoparticles. RSC Adv. 5, 14425.

Banerjee, S., Sharma, G.C., Chattopadhyaya, M.C., Sharma, Y.C., 2014. Kinetic and equilibrium modeling for the adsorptive removal of methylene blue from aqueous solutions on activated fly ash (AFSH). J. Environ. Chem. Eng. 2, 1870.

Bahaabad, M.S., Nassaj, E.T., 2008. Economical synthesis of nano alumina powder using an aqueous sol–gel method. Mater. Lett. 62, 3364.

Barret, E.P., Joyner, L.G., Halenda, P.P., 1951. The determination of pore volume and area distributions in porous substances. I. Computations from nitrogen isotherms. J. Am. Chem. Soc. 73, 373.

Bird, C.L., 2012. The dyeing of wool. In: Asquith, R.S. (Ed.), Chemistry of Natural Protein Fibers. Springer, New York, pp. 310–330.

Brame, J., Li, Q., Alvarez, P.J.J., 2011. Nanotechnology enabled water treatment and reuse: emerging opportunities and challenges for developing countries. Trends Food Sci. Technol. 22, 618.

Busca, G., Lorenzelli, V., Ramis, G., Willeyi, R.J., 1993. Surface sites on spinel-type and corundum-type metal oxide powders. Langmuir 9, 1492.

Cooney, D.O., 1993. Comparison of simple adsorber breakthrough curve method with exact solution. AIChE J. 30, 355.

Crank, J., 1975. The Mathematics of Diffusion. Clarendon Press, London.

Cai, W., Hu, Y., Yu, J., Wang, W., Zhou, J., Jaroniec, M., 2015. Template-free synthesis of hierarchical γ-Al_2O_3 nanostructures and their adsorption affinity toward phenol and CO_2. RSC Adv. 5, 7066.

Dizge, N., Aydiner, C., Demirbas, E., Kobya, M., Kara, S., 2008. Adsorption of reactive dyes from aqueous solutions by fly ash: Kinetic and equilibrium studies. J. Hazard. Mater. 150, 737.

Dotto, G.L., Buriol, C., Pinto, L.A.A., 2014. Diffusional mass transfer model for the adsorption of food dyes on chitosan films. Chem. Eng. Res. Des. 92, 2324.

Dubinin, M.M., Radushkevich, L.V., 1947. The equation of the characteristic curve of the activated charcoal. Proc. Acad. Sci. USSR Phys. Chem. Sect. 55, 331.

Dabrowski, A., 2001. Adsorption–from theory to practice. Adv. Colloid Interf. Sci. 93, 135.

Freundlich, H.M.F., 1906. Uber die adsorption in losungen. J. Phys. Chem. 57, 385.

Gautam, R.K., Gautam, P.K., Banerjee, S., Soni, S., Singh, S.K., Chattopadhyaya, M.C., 2015. Removal of Ni(II) by magnetic nanoparticles. J. Mol. Liq. 204, 60.

Ghaedi, M., Tavallali, H., Sharifi, M., Kokhdan, S.N., Asghari, A., 2012. Preparation of low cost activated carbon from Myrtuscommunis and pomegranate and their efficient application for removal of Congo red from aqueous solution. Spectrochim. Acta Part A Mol. Biomol. Spectrosc. 86, 107.

Giles, D.E., Mohapatra, M., Issa, T.B., Anand, S., Singh, P., 2011. Iron and aluminium based adsorption strategies for removing arsenic from water. J. Environ. Manage. 92, 3011.

He, S., Han, C., Wang, H., Zhu, W., He, S., He, D., Luo, Y., 2015. Uptake of arsenic (V) using alumina functionalized highly ordered mesoporous SBA-15 (Al_x-SBA-15) as an effective adsorbent. J. Chem. Eng. Data 60, 1300.

Ho, Y.S., McKay, G., 1999. Pseudo-second order model for sorption processes. Process Biochem. 14, 451.

Hordern, B.K., 2004. Chemistry of alumina, reactions in aqueous solution and its application in water treatment. Adv. Colloid Interf. Sci. 110, 19.

Huang, B., Bartholomew, C.H., Smith, S.J., Woodfield, B.F., 2013. Facile solvent-deficient synthesis of mesoporous γ-alumina with controlled pore structures. Microporous Mesoporous Mater. 165, 70.

Isfahani, T.D., Javadpour, J., Khavandi, A., Dinnebier, R., Goodarzi, M., Rezaie, H.R., 2012. Mechanochemical synthesis of alumina nanoparticles: formation mechanism and phase transformation. Powder Technol. 229, 17.

Lagergren, S., 1898. About the theory of so-called adsorption of soluble substances. K. Sven. Vetenskpsakad. Handl. 24, 1.

Langmuir, I., 1918. The adsorption of gases on plane surfaces of glass, mica and platinum. J. Am. Chem. Soc. 40, 1361.

Li, L., Fan, M., Brown, R.C., Leeuwen, J.V., Wang, J., Wang, W., Song, Y., Zhang, P., 2006. Synthesis, properties, and environmental applications of nanoscale iron-based materials: a review. Crit. Rev. Environ. Sci. Technol. 36, 405.

Li, H., Zhang, L., Dai, H., He, H., 2009. Facile synthesis and unique physicochemical properties of three-dimensionally ordered macroporous magnesium oxide, gamma-alumina, and ceria-zirconia solid solutions with crystalline mesoporous walls. Inorg. Chem. 48, 4421.

Li, W., Cao, C.Y., Wu, L.Y., Ge, M.F., Song, W.G., 2011. Superb fluoride and arsenic removal performance of highly ordered mesoporous aluminas. J. Hazard. Mater. 198, 143.

Li, Y., Bastakoti, B.P., Malgras, V., Li, C., Tang, J., Kim, J.H., Yamauchi, Y., 2015. Polymeric micelle assembly for the smart synthesis of mesoporous platinum nanospheres with tunable pore sizes. Angew. Chem. Int. Ed. 54, 11073.

Malgras, V., Esfahani, H.A., Wang, H., Jiang, B., Li, C., Wu, K.C.W., Kim, J.H., Yamauchi, Y., 2016. Nanoarchitectures for mesoporous metals. Adv. Mater. 28, 993.

Malgras, V., Ji, Q., Kamachi, Y., Mori, Y., Shieh, F., Wu, K.C., Ariga, K., Yamauchi, Y., 2015. Templated synthesis of nanoarchitectured porous materials. Bull. Chem. Soc. Jpn. 88, 1171.

Mohmood, I., Lopes, C.B., Lopes, I., Ahmad, I., Duarte, A.C., Pereira, E., 2013. Nanoscale materials and their use in water contaminants removal—a review. Environ. Sci. Pollut. Res. 20, 1239.

Monash, P., Pugazhenthi, G., 2014. Utilization of calcined Ni-Al layered double hydroxide (LDH) as an adsorbent for removal of methyl orange dye from aqueous solution. Environ. Prog. Sustain. Energy 33, 154.

Patterson, A.L., 1939. The Scherrer Formula for X-ray particle size determination. Phys. Rev. 56, 978.

Piccin, J.S., Dotto, G.L., Vieira, M.L.G., Pinto, L.A.A., 2011. Kinetics and mechanism of the food dye FD&C Red 40 adsorption onto chitosan. J. Chem. Eng. Data 56, 3759.

Porter, J.F., McKay, G., Choy, K.H., 1999. The prediction of sorption from a binary mixture of acidic dyes using single and mixed isotherm variants of the ideal adsorbed solute theory. Chem. Eng. Sci. 54, 5863.

Renuka, N.K., Shijina, A.V., Praveen, A.K., 2012. Mesoporous γ-alumina nanoparticles: synthesis, characterization and dye removal efficiency. Mater. Lett. 82, 42.

Savage, N., Diallo, M.S., 2005. Nanomaterials and water purification: opportunities and challenges. J. Nanoparticle Res. 7, 331.

Shao, Z., Zhou, W., Zhu, Z., 2012. Advanced synthesis of materials for intermediate-temperature solid oxide fuel cells. Prog. Mater. Sci. 57, 804.

Sharma, Y.C., Srivastava, V., Singh, V.K., Kaul, S.N., Weng, C.H., 2009. Nano-adsorbents for the removal of metallic pollutants from water and wastewater. Environ. Tech. 30, 583.

Sharma, Y.C., Srivastava, V., Mukherjee, A.K., 2010. Synthesis and application of nano-Al_2O_3 powder for the reclamation of hexavalent chromium from aqueous solutions. J. Chem. Eng. Data 55, 2390.

Sharma, Y.C., Srivastava, V., Upadhyay, S.N., Weng, C.H., 2008. Alumina nanoparticles for the removal of Ni(II) from aqueous solutions. Ind. Eng. Chem. Res. 47, 8095.

Shek, C.H., Lai, J.K.L., Gu, T.S., Lin, G.M., 1997. Transformation evolution and infrared absorption spectra of amorphous and crystalline nano-AI_2O_3 powders. NanoStruct. Mater. 8, 605.

Shen, S., Ng, W.K., Chia, L.S.O., Dong, Y.C., Tan, R.B.H., 2012. Morphology controllable synthesis of nanostructured boehmite and γ-alumina by facile dry gel conversion. Cryst. Growth Des. 12, 4987.

Srivastava, V., Weng, C.H., Singh, V.K., Sharma, Y.C., 2011. Adsorption of nickel Ions from aqueous solutions by nano alumina: kinetic, mass transfer, and equilibrium studies. J. Chem. Eng. Data 56, 1414.

Tang, J., Salunkhe, R.R., Liu, J., Torad, N.L., Imura, M., Furukawa, S., Yamauchi, Y., 2015. Thermal conversion of core−shell metal−organic frameworks: a new method for selectively functionalized nanoporous hybrid carbon. J. Am. Chem. Soc. 137, 1572.

Tok, A.I.Y., Boey, F.Y.C., Zhao, X.L., 2006. Novel synthesis of Al_2O_3 nano-particles by flame spray pyrolysis. J. Mater. Process. Technol. 178, 270.

Uma, Banerjee, S., Sharma, Y.C., 2013. Equilibrium and kinetic studies for removal of malachite green from aqueous solution by a low cost activated carbon. J. Ind. Eng. Chem. 19, 1099.

Wang, S., Li, X., Wang, S., Li, Y., Zhai, Y., 2008. Synthesis of γ-alumina via precipitation in ethanol. Mater. Lett. 62, 3552.

Wawrzkiewicz, M., Wiśniewska, M., Gunko, V.M., Zarko, V.I., 2015. Adsorptive removal of acid, reactive and direct dyes from aqueous solutions and wastewater using mixed silica–alumina oxide. Powder Technol. 278, 306.

Weber, W.J., Morris, J.C., 1963. Kinetics of adsorption on carbon from solution. J. Sanit. Eng. Div. 89, 31.

Yang, D.J., Paul, B., Xu, W.J., Yuan, Y., Liu, E.M., Ke, X.B., Wellard, R.M., Guo, C., Xu, Y., Sun, Y.H., Zhu, H.Y., 2010. Alumina nanofibers grafted with functional groups: a new design in efficient sorbents for removal of toxic contaminants from water. Water Res. 44, 741.

Yalamaç, E., Trapani, A., Akkurt, S., 2014. Sintering and microstructural investigation of gamma-alpha alumina powders. Eng. Sci. Technol., Int. J. 17, 2.

Zheng, Y.M., Li, N., Zhang, W.D., 2012. Preparation of nanostructured microspheres of Zn–Mg–Al layered double hydroxides with high adsorption property. Colloids Surf. A: Physicochem. Eng. Aspects 415, 195.

Zhou, S., Antonietti, M., Niederberger, M., 2007. Low-temperature synthesis of γ-aluminananocrystals from aluminum acetylacetonate in nonaqueous media. Small 3, 763.